Dark Matter and Leptogenesis Linked by Classical Scale Invariance

Valentin V. Khoze and Alexis D. Plascencia

Institute for Particle Physics Phenomenology, Department of Physics,
Durham University, Durham DH1 3LE, United Kingdom

E-mail: valya.khoze@durham.ac.uk,
a.d.plascencia-contreras@durham.ac.uk

ABSTRACT: In this work we study a classically scale invariant extension of the Standard Model that can explain simultaneously dark matter and the baryon asymmetry in the universe. In our set-up we introduce a dark sector, namely a non-Abelian SU(2) hidden sector coupled to the SM via the Higgs portal, and a singlet sector responsible for generating Majorana masses for three right-handed sterile neutrinos. The gauge bosons of the dark sector are mass-degenerate and stable, and this makes them suitable as dark matter candidates. Our model also accounts for the matter-anti-matter asymmetry. The lepton flavour asymmetry is produced during CP-violating oscillations of the GeV-scale right-handed neutrinos, and converted to the baryon asymmetry by the electroweak sphalerons. All the characteristic scales in the model: the electro-weak, dark matter and the leptogenesis/neutrino mass scales, are generated radiatively, have a common origin and related to each other via scalar field couplings in perturbation theory.

Contents

1 Introduction

The question of why the only scale parameter in the Standard Model (SM) Lagrangian, $-M_{\mathrm{SM}}^2|H|^2$, is much smaller than the Planck scale is at heart of the naturalness problem. The idea of generating a scale radiatively, originally proposed in Ref. [1] can be applied to explain the origin of the electroweak scale in the SM [2, 3]. In this article we will discuss an extension of the Standard Model that addresses some of the main shortcomings of the minimal theory, namely the dark matter (DM), the baryon asymmetry of the universe (BAU) and the origin of the electroweak scale. Our Beyond the Standard Model framework is based on a theory which contains no explicit mass-scale parameters in its tree-level Lagrangian, and all new scales will be generated dynamically at or below the TeV scale. Our specific approach is motivated by the earlier work in Refs. [4–10] and [11, 12]. The idea of generating the electro-weak scale and various scales of new physics via quantum corrections, by starting from a classically scale-invariant theory, has generated a lot of interest. For related studies on this subject we refer the reader to recent papers including Refs. [13–30].

In our set-up we extend the Standard Model by a dark sector, namely a non-Abelian $\mathrm{SU}(2)_{\mathrm{DM}}$ hidden sector that is coupled to the Standard Model via the Higgs portal, and a singlet sector that includes a real singlet σ and three right-handed Majorana neutrinos N_i. Due to an SO(3) custodial symmetry all three gauge bosons Z'^a have the same mass and are absolutely stable, making them suitable dark matter candidates [31] (this also applies to larger gauge groups $\mathrm{SU(N)}_{\mathrm{DM}}$ [32, 33] and to scalar fields in higher representations [34], albeit symmetry breaking patterns get more complicated).

The tree-level scalar potential of our model is given by

$$V_0 = \lambda_\phi |\Phi|^4 + \lambda_h |H|^4 + \frac{\lambda_\sigma}{4}\sigma^4 - \lambda_{h\phi}|H|^2|\Phi|^2 - \frac{\lambda_{\phi\sigma}}{2}|\Phi|^2\sigma^2 + \frac{\lambda_{h\sigma}}{2}|H|^2\sigma^2, \quad (1.1)$$

where Φ denotes the $\mathrm{SU}(2)_{\mathrm{DM}}$ doublet, H is the SM Higgs doublet, and σ is a gauge-singlet introduced in order to generate the Majorana masses for the sterile neutrinos, and hence the visible neutrinos masses and mixings via the see-saw mechanism. The portal couplings $\lambda_{h\phi}$, $\lambda_{\phi\sigma}$ and $\lambda_{h\sigma}$ will play a role in order to induce non-trivial vacuum expectation values for all three scalar. As will become clear from Table 1 we will scan over positive as well as negative values of the portal couplings $\lambda_{h\phi}$ and $\lambda_{h\sigma}$. As we are working with multiple scalars we will adopt the Gildener-Weinberg approach [35], which is a generalisation of the Coleman-Weinberg mechanism to multiple scalar states and will be briefly reviewed in Section 2. Later on we shall see that the most interesting region in parameter space leading to both the correct dark matter abundance and the correct baryon asymmetry is for $\langle\sigma\rangle \gg \langle\phi\rangle$ and hence one can think of σ as a Coleman-Weinberg scalar that once it acquires a non-zero vev it will be communicated to ϕ and h through the portal couplings $\lambda_{\phi\sigma}$ and $\lambda_{h\sigma}$.

The interactions for the right-handed neutrinos in the Lagrangian are given by

$$\mathcal{L}_N = -\frac{1}{2}\left(Y_{ij}^M \sigma \overline{N_i}^c N_j + Y_{ij}^{M\dagger}\sigma\overline{N_i}N_j^c\right) - Y_{ia}^D \,\overline{N_i}(\varepsilon H)l_{La} - Y_{ai}^{D\dagger}\,\overline{l_{La}}(\varepsilon H)^\dagger N_i, \quad (1.2)$$

where the first two term give rise to the Majorana mass once σ acquires a vev, while the last two terms are responsible for the CP-violating oscillations of N_i.

Since we do not wish to break the lepton-number symmetry explicitly, it follows from (1.2) that our new singlet scalar field σ should have the lepton number $L = -2$. We can think of it as the real part of a complex scalar $\Sigma = (\sigma + i\pi)/\sqrt{2}$ where S transforms under a $U(1)_L$ symmetry associated with the lepton number, which is broken spontaneously by $\langle\sigma\rangle \neq 0$. If this is a global $U(1)$ symmetry then there must exist a massless (or very light) (pseudo)-Goldstone boson. Since the Higgs can pair-produce them and decay, this would severely constrain the portal coupling of Σ with the Higgs, $\lambda_{h\sigma} < 10^{-5}$, see e.g. Ref. [5]. If we wish to avoid such fine-tuning, a much more appealing option would be to gauge the lepton number. A compelling scenario is the $B-L$ theory with the anomaly free $U(1)_{B-L}$ factor. The generation of matter-anti-matter asymmetry via a leptogenesis mechanism through sterile neutrino oscillations in a classically-scale-invariant $U(1)_{B-L}\times$SM theory was considered in Ref. [6], and their results will also apply to our model. The main difference with the set-up followed in this paper is that here we allow for a separate non-Abelian Coleman-Weinberg sector (i.e. it remains distinct from the $U(1)_{B-L}$ gauge sector) and as a result we have a non-Abelian vector DM candidate.

Finally, it should also be possible to restrict the complex singlet Σ back to the real singlet σ, just as we have in (1.1). In this case the continuous lepton number $U(1)$ symmetry is reduced to a discrete sub-group:

$$\sigma \to -\sigma, \quad (N, \overline{N}^c, l_L) \to e^{i\pi/2}(N, \overline{N}^c, l_L), \quad (\overline{N}, N^c, \overline{l_L}) \to e^{-i\pi/2}(\overline{N}, N^c, \overline{l_L}). \quad (1.3)$$

In general all three possibilities corresponding to global, local and discrete lepton-number symmetries can be accommodated and considered simultaneously in the context of Eqs. (1.1)-(1.2) by either working with the real scalar σ or the complex one by promoting $\sigma \to \sqrt{2}\Sigma$ (or $\sqrt{2}\Sigma^\dagger$ in the second term in the brackets on the r.h.s. of (1.2)). In this work we consider σ to be a real scalar singlet.

2 From Coleman-Weinberg to the Gildener-Weinberg mechanism

The scalar field content of our model consists of an $SU(2)_L$ doublet H, an $SU(2)_{DM}$ doublet Φ and a real scalar σ; the latter giving mass to the sterile neutrinos after acquiring a vev in similar fashion to Ref. [10]. Working in the unitary gauge of the $SU(2)_L \times SU(2)_{DM}$, the two scalar doublets in the theory are reduced to,

$$H = \frac{1}{\sqrt{2}} \begin{pmatrix} 0 \\ h \end{pmatrix}, \qquad \Phi = \frac{1}{\sqrt{2}} \begin{pmatrix} 0 \\ \phi \end{pmatrix},$$

and the tree-level potential becomes,

$$V_0 = \frac{\lambda_h}{4} h^4 + \frac{\lambda_\phi}{4} \phi^4 + \frac{\lambda_\sigma}{4} \sigma^4 - \frac{\lambda_{h\phi}}{4} h^2 \phi^2 - \frac{\lambda_{\phi\sigma}}{4} \phi^2 \sigma^2 + \frac{\lambda_{h\sigma}}{4} h^2 \sigma^2 \,. \tag{2.1}$$

There are no mass scales appearing in the classical theory, and at the origin in the field space, all scalar vevs are zero, in agreement with classical scale invariance. We impose a conservative constraint on all the scalar couplings for the model to be perturbative $|\lambda_i| < 3$, we also impose $g_{DM} < 3$ and in order to ensure vacuum stability the following set of constraints need to be satisfied,

$$\lambda_h \geq 0, \qquad \lambda_\phi \geq 0, \qquad \lambda_\sigma \geq 0, \tag{2.2}$$

$$\frac{\lambda_{h\phi}}{2\sqrt{\lambda_h \lambda_\phi}} \leq 1, \quad -\frac{\lambda_{h\sigma}}{2\sqrt{\lambda_h \lambda_\sigma}} \leq 1, \quad \frac{\lambda_{\phi\sigma}}{2\sqrt{\lambda_\phi \lambda_\sigma}} \leq 1, \tag{2.3}$$

$$\frac{\lambda_{h\phi}}{2\sqrt{\lambda_h \lambda_\phi}} - \frac{\lambda_{h\sigma}}{2\sqrt{\lambda_h \lambda_\sigma}} + \frac{\lambda_{\phi\sigma}}{2\sqrt{\lambda_\phi \lambda_\sigma}} \leq 1. \tag{2.4}$$

For more detail we refer to Table 1.

2.1 The Coleman-Weinberg approximation

For simplicity, let us temporarily ignore the singlet σ and concentrate on the theory with two scalars, ϕ and h. We will further refer to the hidden $SU(2)_{DM}$ sector with ϕ as the Coleman-Weinberg (CW) sector. In the near-decoupling limit, $\lambda_{h\phi} \ll 1$, between the CW and the SM sectors, we can view electroweak symmetry breaking effectively as a two-step process [5].

First, the CW mechanism [1] generates $\langle \phi \rangle$ in the hidden sector through running couplings (or more precisely the dimensional transmutation). To make this work, the scalar self-coupling λ_ϕ at the relevant scale $\mu = \langle \phi \rangle$ should be small – of the order of $g_{DM}^4 \ll 1$, as

we will see momentarily. This has the following interpretation: in a theory where λ_ϕ has a positive slope, we start at a relatively high scale where λ_ϕ is positive and move toward the infrared until approach the value of the μ where $\lambda_\phi(\mu)$ becomes small and is about to cross zero. This is the Coleman-Weinberg scale where the potential develops a non-trivial minimum and ϕ generates a non-vanishing vev.

To see this, consider the 1-loop effective potential evaluated at the scale μ (*cf.* [9]):

$$V(\phi, h) = \frac{\lambda_\phi(\mu)}{4}\phi^4 + \frac{9}{1024\,\pi^2}\,g_{\mathrm{DM}}^4(\mu)\,\phi^4\left(\log\frac{\phi^2}{\mu^2} - \frac{25}{6}\right) - \frac{\lambda_{h\phi}(\mu)}{4}h^2\phi^2\,, \qquad (2.5)$$

Here we are keeping 1-loop corrections arising from interactions of ϕ with the $SU(2)$ gauge bosons in the hidden sector, but neglecting the loops of ϕ (since λ_ϕ is close to zero) and the radiative corrections from the Standard Model sector. The latter would produce only subleading corrections to the vevs. Minimising at $\mu = \langle\phi\rangle$ gives:

$$\lambda_\phi = \frac{33}{256\,\pi^2}\,g_{\mathrm{DM}}^4 + \lambda_{h\phi}\frac{v^2}{2\langle\phi\rangle^2} \qquad \text{at} \quad \mu = \langle\phi\rangle\,. \qquad (2.6)$$

For small portal coupling $\lambda_{h\phi}$, this is a small deformation of the original CW condition, $\lambda_\phi(\langle\phi\rangle) = \frac{33}{256\,\pi^2}\,g_{\mathrm{DM}}^4(\langle\phi\rangle)$.

The second step of the process is the transmission of the vev $\langle\phi\rangle$ to the Standard Model via the Higgs portal, generating a negative mass squared parameter for the Higgs $= -\lambda_{h\phi}\langle\phi^2\rangle$ which generates the electroweak scale v,

$$v = \langle h\rangle = \sqrt{\frac{2\lambda_{h\phi}}{\lambda_h}}\,\langle\phi\rangle\,, \quad m_h = \sqrt{2\lambda_h}v\,. \qquad (2.7)$$

The fact that for $\lambda_{h\phi} \ll 1$ the generated electroweak scale is much smaller than $\langle\phi\rangle$, guarantees that any back reaction on the hidden sector vev $\langle\phi\rangle$ is negligible. Finally, the mass of the CW scalar is obtained from the 1-loop potential and reads:

$$m_\phi^2 = \frac{9}{128\,\pi^2}\,g_{\mathrm{DM}}^4\,\langle\phi\rangle^2 + \lambda_{h\phi}v^2\,. \qquad (2.8)$$

As already stated, this approach is valid in the near-decoupling approximation where all the portal couplings are small. The dynamical generation of all scales is visualised here as first the generation of the CW scalar vev $\langle\phi\rangle$, which then induces the vevs of other scalars proportional to the square root of the corresponding portal couplings $\ll 1$, as in (2.7). This implies the hierarchy of the vevs.

For multiple scalars, ϕ, h and σ, it is not a priori obvious why the portal couplings should be small and which of the scalar vevs should be dominant. For example on one part of the parameter space we can find $\langle\phi\rangle > \langle\sigma\rangle$ and on a different part one has $\langle\sigma\rangle > \langle\phi\rangle$ (so that σ rather than ϕ effectively plays the role of the CW scalar). To consider all such cases and not be constrained by the near-decoupling limits we will utilise the Gildener-Weinberg set-up [35], which is a generalization of the Coleman-Weinberg method.

2.2 The Gildener-Weinberg approach

We now return to the general case with the three scalars in the model are described by the tree-level massless scalar potential (2.1). The Gildener-Weinberg mechanism was recently worked out for this case in Ref. [10], which we will follow. All three vevs can be generated dynamically but neither of the original scalars is solely responsible for the intrinsic scale generation; this instead is a collective effect generated by a linear combination of all three scalars φ.

Following [35], we change variables and reparametrise the scalar fields via,

$$h = N_1\varphi, \quad \phi = N_2\varphi, \quad \sigma = N_3\varphi. \tag{2.9}$$

where each N_i is a unit vector in three-dimensions. The Gildener-Weinberg mechanism tells us that a non-zero vacuum expectation value will be generated in some direction in scalar field space $N_i = n_i$, so this direction must satisfy the condition,

$$\left. \frac{\partial V_0}{\partial N_i} \right|_{\mathbf{n}} = 0, \tag{2.10}$$

and furthermore the value of the tree-level potential in this vacuum is independent of φ,

$$V_0(n_1\varphi, n_2\varphi, n_3\varphi) = 0. \tag{2.11}$$

The latter condition is simply the statement that the potential restricted to the single degree of freedom φ, is of the form $\frac{1}{4}\lambda_\varphi \varphi^4$ with the corresponding coupling constant vanishing $\lambda_\varphi = 0$. This is nothing but the definition of scale μ_{GW} where $\lambda_\varphi(\mu_{\mathrm{GW}})$ vanishes, and is a reflection of a similar statement in the Coleman-Weinberg case for the single scalar that its self-coupling was about to cross zero, but was stabilised at the small positive value by the gauge coupling at the Coleman-Weinberg scale μ_{CW}, see Eq. (2.6).

Being a unit vector in three-dimensions, n_i's can be parametrised in terms of two independent angles, α and γ and we will call the φ vev, w, so that,

$$n_1 = \sin\alpha, \quad n_2 = \cos\alpha\cos\gamma \quad n_3 = \cos\alpha\sin\gamma, \tag{2.12}$$
$$\langle h \rangle = wn_1, \quad \langle \phi \rangle = wn_2, \quad \langle \sigma \rangle = wn_3. \tag{2.13}$$

The three linearly-independent conditions arising from the Gildener-Weinberg minimisation (2.10) of the tree-level potential amount to the following set of relations,

$$2\lambda_h n_1^2 = \lambda_{h\phi} n_2^2 - \lambda_{h\sigma} n_3^2, \tag{2.14}$$
$$2\lambda_\phi n_2^2 = \lambda_{h\phi} n_1^2 + \lambda_{\phi\sigma} n_3^2, \tag{2.15}$$
$$2\lambda_\sigma n_3^2 = \lambda_{\phi\sigma} n_2^2 - \lambda_{h\sigma} n_1^2. \tag{2.16}$$

These conditions hold at the scale μ_{GW} where the scalar fields develop the vev $\langle \varphi \rangle = w$ (2.13). Due to the three scalars acquiring non-zero vacuum expectation values, the three

states will mix among each other. The mass matrix M^2 is diagonalised for h_1, h_2 and h_3 eigenstates via the rotation matrix O,

$$\text{diag}\left(M_{h_1}^2, M_{h_2}^2, M_{h_3}^2\right) = O^{(-1)} M^2 O, \qquad \begin{pmatrix} h \\ \phi \\ \sigma \end{pmatrix} = O_{ij} \begin{pmatrix} h_1 \\ h_2 \\ h_3 \end{pmatrix}, \qquad (2.17)$$

and we further identify the state h_1 with the SM 125 GeV Higgs boson. Following [10] we parametrise the rotation matrix in terms of three mixing angles α, β and γ,

$$O = \begin{pmatrix} \cos\alpha\cos\beta & \sin\alpha & \cos\alpha\sin\beta \\ -\cos\beta\cos\gamma\sin\alpha + \sin\beta\sin\gamma & \cos\alpha\cos\gamma & -\cos\gamma\sin\alpha\sin\beta - \cos\beta\sin\gamma \\ -\cos\gamma\sin\beta - \cos\beta\sin\alpha\sin\gamma & \cos\alpha\sin\gamma & \cos\beta\cos\gamma - \sin\alpha\sin\beta\sin\gamma \end{pmatrix},$$
$$(2.18)$$

and use it to compute the scalar mass eigenstates (2.17) at tree-level. The resulting expressions for the scalar masses can be found in Ref. [10]. There is one classically flat direction in the model – along φ – in which the potential develops the vacuum expectation value. Our choice of parametrisation in (2.13) and in the second row of (2.18) in terms of the same two angles α and γ, selects this direction to be identified with h_2. Hence, at tree level, $M_{h_2} = 0$, but it will become non-zero, see Eq. (2.22) below, when one-loop effects are included.

At the scale μ_{GW} the one-loop effective potential along the minimum flat direction can be written as [35],

$$V(\varphi\mathbf{n}) = A\varphi^4 + B\varphi^4 \log\left(\frac{\varphi^2}{\mu_{\text{GW}}^2}\right), \qquad (2.19)$$

where the A and B coefficients are computed in the $\overline{\text{MS}}$ [36] scheme and given by,

$$A = \frac{1}{64\pi^2 w^4}\left[\sum_{i=1,3} M_{h_i}^4\left(-\frac{3}{2} + \log\frac{M_{h_i}^2}{w^2}\right) + 6M_W^4\left(-\frac{5}{6} + \log\frac{M_W^2}{w^2}\right) + 3M_Z^4\left(-\frac{5}{6} + \log\frac{M_Z^2}{w^2}\right)\right.$$
$$\left. + 9M_{Z'}^4\left(-\frac{5}{6} + \log\frac{M_{Z'}^2}{w^2}\right) - 12M_t^4\left(-1 + \log\frac{M_t^2}{w^2}\right) - 2\sum_{i=1}^3 M_{N_i}^4\left(-1 + \log\frac{M_{N_i}^2}{w^2}\right)\right],$$

$$B = \frac{1}{64\pi^2 w^4}\left(\sum_{i=1,3} M_{h_i}^4 + 6M_W^4 + 3M_Z^4 + 9M_{Z'}^4 - 12M_t^4 - 2\sum_{i=1}^3 M_{N_i}^4\right),$$

where M_{h_i} are the tree-level masses of the three scalar eigenstates, h_1, h_2 and h_3, and the rest are the masses of the SM and the hidden sector vector bosons as well as the top quark and the right-handed Majorana neutrinos. We can now see that at the RG scale μ_{GW} the 1-loop corrected effective potential has a fixed vacuum expectation value w that satisfies,

$$\log\left(\frac{w}{\mu_{\text{GW}}}\right) = -\frac{1}{4} - \frac{A}{2B}, \qquad (2.20)$$

and using this relation we can rewrite the one-loop effective potential as,

$$V = B\varphi^4\left(\log\frac{\varphi^2}{w^2} - \frac{1}{2}\right), \qquad (2.21)$$
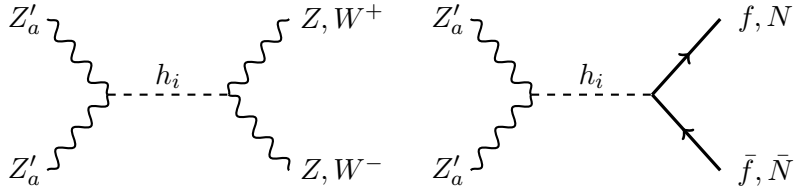
Figure 1: Dark matter annihilation diagrams into Standard Model gauge bosons and fermions, we also include annihilation into right-handed neutrinos.
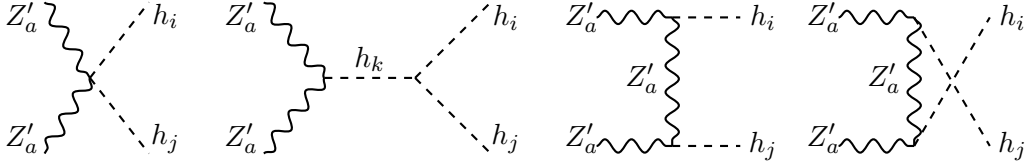
Figure 2: Dark matter annihilation diagrams into scalar states.
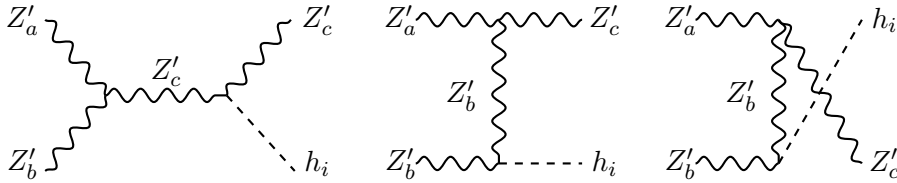
Figure 3: Vector dark matter semi-annihilation diagrams. In contrast to some other models of dark matter, Z'_a is stable due to an remnant global symmetry.

and we can also evaluate the potential at the minimum to be $V(\varphi = w) = -Bw^4/2$, which gives the requirement $B > 0$ for this to be a lower minimum than the one at the origin. The mass of the pseudo-dilaton h_2 is then given by,

$$M_{h_2}^2 = \frac{\partial^2 V}{\partial \varphi^2}\bigg|_{\mathbf{n}} = \frac{1}{8\pi w^2}\left(M_{h_1}^4 + M_{h_3}^4 + 6M_W^4 + 3M_Z^4 + 9M_{Z'}^4 - 12M_t^4 - 2\sum_{i=1}^{3}M_{N_i}^4\right). \tag{2.22}$$

In summary, at the scale μ_{GW} the conditions Eqs. (2.14)–(2.16) will be satisfied and the scalar potential will develop a non-trivial vev w giving rise to non-zero vacuum expectation values $\langle h \rangle$, $\langle \phi \rangle$, and $\langle \sigma \rangle$. For one scalar field, the Coleman-Weinberg mechanism requires the scalar quartic coupling to take very small values $\lambda_\phi \sim g_{\mathrm{DM}}^4$, in the Gildener-Weinberg scenario it is a combination of the quartic couplings that needs to vanish, so these couplings can take larger values individually.

The formulae for the mixing angles in terms of the coupling constants and the vevs

follow from the diagonalisation of the tree-level mass matrix,

$$\tan^2 \alpha = \frac{\langle h \rangle^2}{\langle \phi \rangle^2 + \langle \sigma \rangle^2} = \frac{4\lambda_\phi \lambda_\sigma - \lambda_{\phi\sigma}^2}{2(\lambda_\sigma \lambda_{h\phi} - \lambda_\phi \lambda_{h\sigma}) + \lambda_{\phi\sigma}(\lambda_{h\phi} - \lambda_{h\sigma})} \,, \tag{2.23}$$

$$\tan^2 \gamma = \frac{\langle \sigma \rangle^2}{\langle \phi \rangle^2} = \frac{2\lambda_h \lambda_{\phi\sigma} - \lambda_{h\phi}\lambda_{h\sigma}}{4\lambda_h \lambda_\sigma - \lambda_{h\sigma}^2} \,, \tag{2.24}$$

$$\tan 2\beta = \frac{\langle h \rangle \langle \phi \rangle \langle \sigma \rangle \, w (\lambda_{h\sigma} + \lambda_{h\phi})}{(\lambda_\phi + \lambda_\sigma + \lambda_{\phi\sigma})\langle \phi \rangle^2 \langle \sigma \rangle^2 - \lambda_h \langle h \rangle^2 w^2} \,. \tag{2.25}$$

Experimental searches of a scalar singlet mixing with the SM Higgs provide constraints on the mixing angles [37–39]. In our case, these translate as,

$$\cos^2 \alpha \, \cos^2 \beta > 0.85. \tag{2.26}$$

In the region where the decay $h_1 \to h_2 h_2$ is allowed we impose the stronger constraint $\cos^2 \alpha \cos^2 \beta > 0.96$. Nonetheless, due to the Gildener-Weinberg conditions the decay $h_1 \to h_2 h_2$ is highly suppressed. In the scan we perform M_{h_3} is always greater than M_{h_1}, so there is no need to worry about the SM Higgs decaying into two h_3 scalars. At the same time, strong constraints could come when the decays $h_1 \to Z'^a Z'^a$ are allowed, we set $M_{Z'} > M_{h_1}/2$ so that these decays are kinematically forbidden.

For the study of dark matter the Lagrangian contains ten dimensionless free parameters, which are reduced to eight after fixing $\langle h \rangle = 246$ GeV and $M_{h_1} = 125$ GeV. We perform a random scan on the remaining eight parameters in the ranges given in Table 1.

Parameter	Scan range
$\lambda_{\phi\sigma}$	(0, 0.5)
$\lambda_{h\phi}$	(-0.5, 0.5)
$\lambda_{h\sigma}$	(-0.25, 0.25)
λ_ϕ	(0, 3)
$g_{\rm DM}$	(0, 3)
M_{N_i}	(0, 100) GeV

Table 1: Ranges for the input parameters in the scan.

The matrix Y^D has no impact on the dark matter phenomenology, but it is crucial for Leptogenesis and it will be parametrised by three complex angles ω_{ij} using the Casas-Ibarra parametrisation [40]. Therefore, once we set all the parameters for the active neutrinos to their best experimental fit, there are twelve free parameters in the model.

3 Dark matter phenomenology

Evidence from astrophysics suggests that most of the matter in the universe is made out of cosmologically stable dark matter that interacts very weakly with ordinary matter. Being able to identify what constitutes this dark matter is one of the deepest mysteries in both
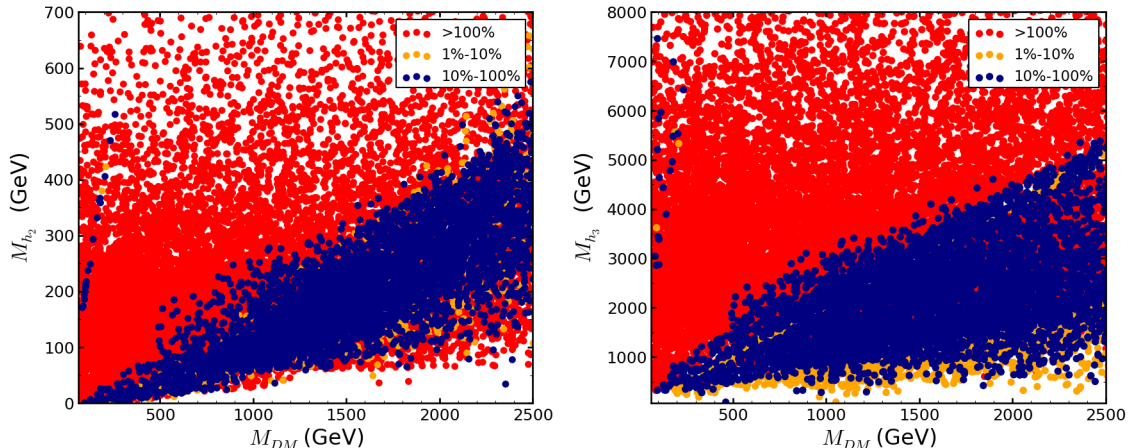
Figure 4: Left panel shows scatter plot of the dark matter mass $M_{\mathrm{DM}} = M_{Z'}$ versus the scalar mass M_{h_2}. Right panel gives scatter plot of the dark matter mass versus the mass of the heavier scalar h_3. Different colours indicate whether the vector gauge triplet accounts for more or less than 100%, 10% and 1% of the observed dark matter abundance.

particle physics and astrophysics. In this work we consider the possibility of dark matter being a spin-1 particle from a hidden sector with non-Abelian $\mathrm{SU}(2)_{\mathrm{DM}}$ gauged symmetry. The idea of vector dark matter was first introduced in Ref. [31] and later studied in Refs. [7, 9, 32, 41]. Note that if the hidden sector had been U(1), the kinetic mixing among the hidden sector and the hypercharge will have made our dark matter candidate unstable.

After radiative symmetry breaking breaking of $\mathrm{SU}(2)_{\mathrm{DM}}$ by Φ, which is in the fundamental representation of the group, there is a remnant SO(3) symmetry that ensures the three gauge bosons Z'^a acquire the same mass $M_{Z'} = \frac{1}{2} g_{\mathrm{DM}} \langle \phi \rangle$, and are stable. In contrast to models where the DM is odd under a $\mathbb{Z}_2$ discrete symmetry, in the present scenario we can have dark matter semi-annihilation processes where a DM particle is also present in the final state. The DM annihilation diagrams are shown in Figs. 1 and 2, while the semi-annihilation ones are shown in Fig. 3.

Also, due to the radiative generation of $\langle \phi \rangle$ in most region of parameter space the scalar mass will be smaller than the gauge boson mass, $M_{h_2} < M_{Z'}$. This means that semi-annihilation processes $Z'^a Z'^b \to Z'^c h_i$ will be dominant over annihilation ones in most of the parameter space. To leading order the non-relativistic cross-section from the semi-annihilation diagrams is given by (*cf.* [9]),

$$\langle \sigma_{abc} v \rangle = \frac{3 g_{\mathrm{DM}}^4}{128\pi} \frac{(O_{2i})^2}{M_{Z'}^2} \left(1 - \frac{M_{h_i}^2}{3 M_{Z'}^2} \right)^{-2} \left(1 - \frac{10 M_{h_i}^2}{9 M_{Z'}^2} + \frac{M_{h_i}^4}{9 M_{Z'}^4} \right)^{3/2} . \tag{3.1}$$

In order to take into account all annihilation channels into SM particles and properly take into account thresholds and resonances we have implemented the model in `microMEGAs 4.1.5` [42]. We fix the dark matter relic abundance from the latest Planck satellite mea-
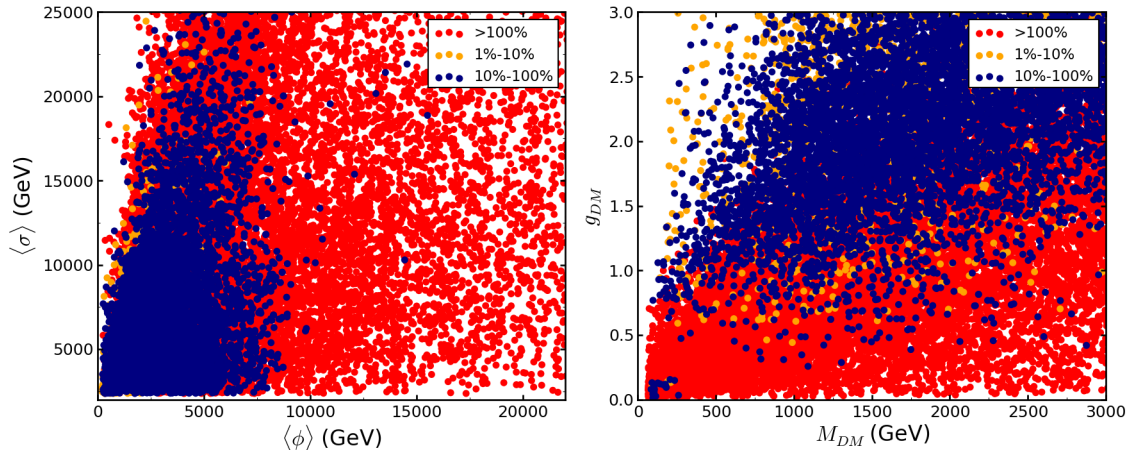
Figure 5: Left panel: Scatter plot of the vev $\langle\phi\rangle$ versus the vev of the scalar singlet $\langle\sigma\rangle$. Due to the small mixing angles, we can see that the dark matter relic density is almost independent of $\langle\sigma\rangle$. Right panel: Scatter plot of the dark matter mass $M_{Z'}$ versus the gauge coupling $g_{\rm DM}$. Different colours indicate whether the vector gauge triplet accounts for more or less than 100%, 10% and 1% of the observed dark matter abundance.
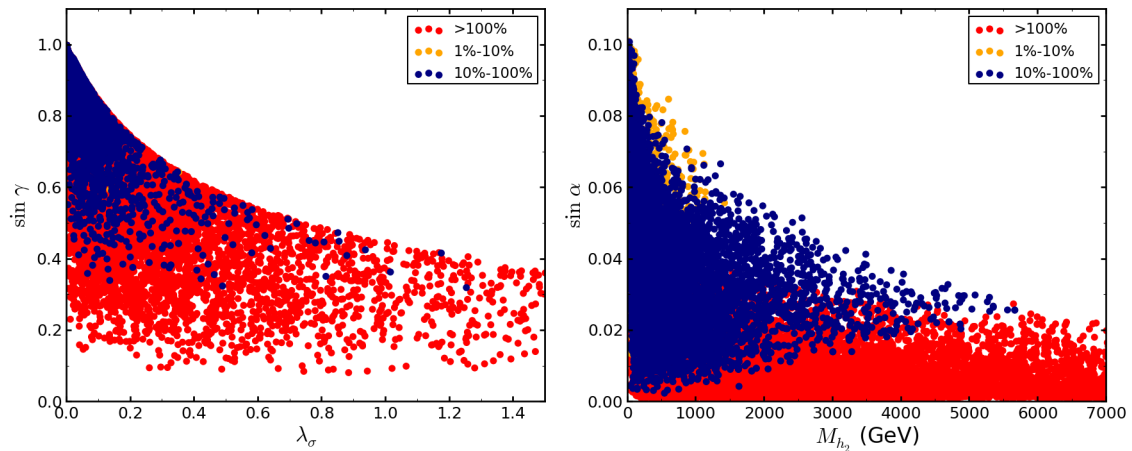
Figure 6: Left panel: Scatter plot of $\sin\gamma$ against the quartic coupling λ_σ. Larger values of $\sin\gamma$ are preferred. Right panel: Scatter plot of $\sin\alpha$ versus the scalar mass M_{h_2}. Due to $\langle\sigma\rangle \gg \langle h\rangle$ we get small values for the mixing angle α. Different colours indicate whether the vector gauge triplet accounts for more or less than 100%, 10% and 1% of the observed dark matter abundance.

surement $\Omega h^2 = 0.1197 \pm 0.0022$ [43]. Figure 4 shows the dark matter fraction as a function of $M_{Z'}$ and the scalar mass M_{h_2}; the isolated strip of points on the left side of the plots corresponds to the resonance $M_{h_2} \approx 2M_{Z'}$.
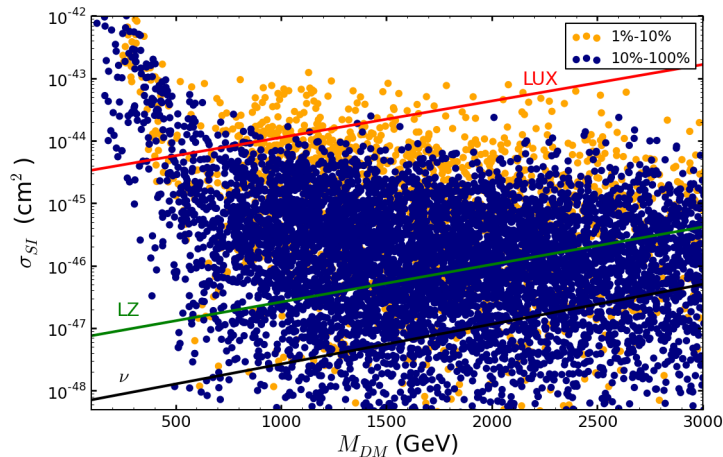
Figure 7: Spin-independent DM-nucleon cross section as a function of the DM candidate mass $M_{Z'}$. We show current experimental limits from LUX [44] (red line), future limits from LZ [45] (green line) and the neutrino coherent scattering limit [46] (black line).

On the left plot in Fig. 4 there is a large red coloured region on the left side (producing too much dark matter), in this region M_{h_2} has a close value to $M_{Z'}$ (note that this region does not exist in the Coleman-Weinberg limit). This region exists thanks to very large values of M_{h_3} and $\langle\phi\rangle \gg M_{Z'}$. In the left panel of Fig. 5 we show the dark matter fraction as a function of both vevs, $\langle\phi\rangle$ and $\langle\sigma\rangle$, from this plot we see there is an upper bound on $\langle\phi\rangle$ in order not to overproduce dark matter, $\langle\phi\rangle < 17$ TeV. Later on we shall see that there is a lower bound on $\langle\sigma\rangle$ coming from leptogenesis, $\langle\sigma\rangle > 2.5$ TeV, we have already imposed this bound on all the scatter plots we show.

In the right panel of Fig. 5 we show the dark matter fraction as a function of $M_{Z'}$ and the gauge coupling g_{DM}. In this plot it becomes clear that as we increase the gauge coupling, the relic density decreases. The left panel of Fig. 6 shows the same analysis for the mixing angle $\sin\gamma$ and the quartic couplng λ_σ. Here we can already notice a preference for the region $\sin\gamma \approx 1$, where λ_σ takes on small values and $\langle\sigma\rangle \gg \langle\phi\rangle$. Due to the lower bound on $\langle\sigma\rangle$ the mixing angle α takes on very small values, this is shown in the right panel of Fig. 6.

The spin-independent cross section between Z'^a and a nucleon is given by,

$$\sigma_{\text{SI}} = \frac{f_N^2 \, m_N^4 \, M_{Z'}^2}{\pi \, \langle h \rangle^2 \, \langle \phi \rangle^2} \left(\sum_{i=1}^{3} \frac{O_{2i} O_{1i}}{M_{h_i}^2} \right)^2, \tag{3.2}$$

where m_N is the nucleon mass, $f_N = 0.303$ [33] is the nucleon form-factor, and O_{ij} are the elements of the rotation matrix Eq. (2.18) that relates the scalar mass eigenstates states to the ones in the Lagrangian. This orthogonal matrix O is the one that diagonalises the mass matrix. Due to the form of this matrix, the direct detection diagrams have a destructive interference when the scalar state with a large ϕ component has a mass very close to M_{h_1}, this has been previously noted in [7, 47]; while the scalar state with a large σ component
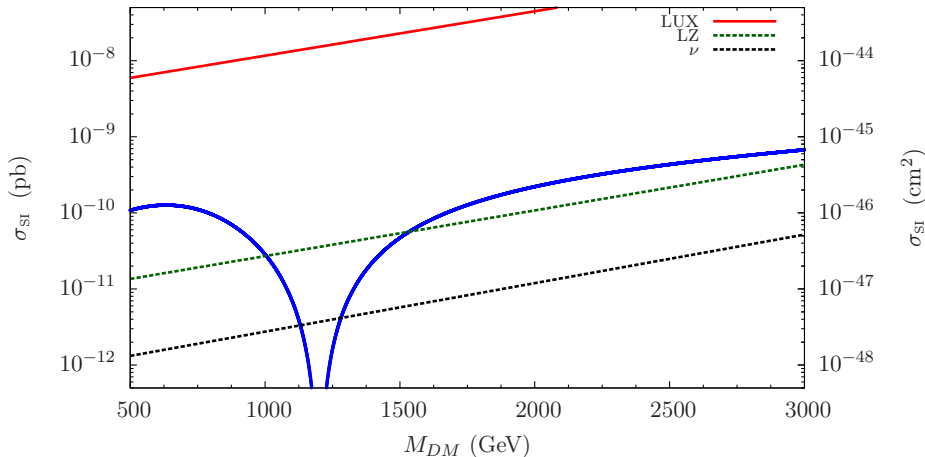
Figure 8: Spin-independent DM-nucleon cross section as a function of the vector DM candidate mass $M_{Z'}$, for benchmark point BP 1. We show current experimental limits from LUX [44] (red line), future limits from LZ [45] (green line) and the neutrino coherent scattering limit [46] (black line). To generate this plot we fix all the scalar couplings and vary only g_{DM}, which means that $M_{Z'}$ and M_{h_2} are also varied while all other parameters remain fixed.

has no direct couplings either to dark matter or to Standard Model particles and hence gives only a small contribution to σ_{SI}. Figure 7 shows that except for resonances, the region with $M_{Z'} < 250$ GeV has been already excluded by the existing experiments, while a large region of parameter space will be tested by future underground experiments such as LZ [45] and XENON1T [48]. In Fig. 8 we show the direct-detection cross section as a function of the dark matter mass for benchmark point BP 1, we fix all the scalar couplings and vary only g_{DM}, the dip corresponds to $M_{h_2} \approx M_{h_1}$.

4 Leptogenesis via oscillations of right-handed neutrinos

Leptogenesis is an attractive and minimal mechanism to solve the baryon asymmetry of the universe (BAU). This means being able to produce the observed value of

$$\frac{n_{b_{\mathrm{obs}}}}{s} = (8.75 \pm 0.23) \times 10^{-11}. \tag{4.1}$$

In the Akhmedov-Rubakov-Smirnov framework [11] a lepton flavour asymmetry is produced during oscillations of the right-handed Majorana neutrinos N_i with masses around the electroweak scale or below, which makes this approach compatible with classical scale invariance.[1] From Big Bang nucleosynthesis we obtain the lower bound $M_N > 200$ MeV, in

---

[1]In the sense that no additional very large scales are required to be introduced in the model to make this type of leptogenesis work.

order not to spoil primordial nucleosynthesis. For our calculations we make use of the the Casas-Ibarra parametrisation [40] for the matrix Y^D,

$$Y^{D\,\dagger} = U_\nu \cdot \sqrt{m_\nu} \cdot \mathcal{R} \cdot \sqrt{M_N} \times \frac{\sqrt{2}}{\langle h \rangle} \,, \tag{4.2}$$

where m_ν and M_N are diagonal mass matrices of active and Majorana neutrinos respectively. The active-neutrino-mixing matrix U_ν is the PMNS matrix which contains six real parameters, including three measured mixing angles and three CP-phases. The matrix $\mathcal{R}$ is parametrised by three complex angles ω_{ij}. Using this framework with three right-handed neutrinos one can generate the correct baryon asymmetry without requiring tuning the N_i mass splittings, but rather enhancing the entries in the Dirac Yukawa matrix through the imaginary parts of the complex angles ω_{ij} [49].

Due to the non-trivial topological structure of the vacuum in $SU(2)_L$ there exist electroweak sphaleron processes which violate $B + L$ quantum number, and these will transfer the lepton flavour asymmetry n_{Le} into a baryon asymmetry n_b, with the conversion factor given by,

$$\frac{n_b}{s} \simeq -\frac{3}{14} \times 0.35 \times \frac{n_{Le}}{s}. \tag{4.3}$$

A critical condition for the mechanism of [11] to work, is that two of three neutrino flavours, N_2 and N_3, should come into thermal equilibrium with their Standard Model counterparts before the universe cools down to $T_{\rm EW}$ (when electroweak sphaleron processes freeze out), while the remaining flavour does not. In other words, the present mechanism consists of different time scales $T_{\rm osc} \gg T_{eq_3} \sim T_{eq_2} > T_{\rm EW} > T_{eq_1}$, where T_{eq_i} represents the temperature at which N_i equilibrates with the thermal plasma and $T_{\rm osc}$ is the temperature at which the oscillations start to occur. In terms of the decay rates for the three sterile neutrino flavours this implies,

$$\Gamma_2(T_{\rm EW}) > H(T_{\rm EW}) \,, \quad \Gamma_3(T_{\rm EW}) > H(T_{\rm EW}) \,, \quad \Gamma_1(T_{\rm EW}) < H(T_{\rm EW}), \tag{4.4}$$

where H is the Hubble constant,

$$H(T) = \frac{T^2}{M_{\rm P}^*} \,, \qquad M_{\rm P}^* \equiv \frac{M_{\rm P}}{\sqrt{g_*}\sqrt{4\pi^3/45}} \simeq 10^{18}\,{\rm GeV} \tag{4.5}$$

and $M_{\rm P}^*$ is the reduced Planck mass. Therefore, we require,

$$\Gamma_1(T_{\rm EW}) = \frac{1}{2} \sum_i Y_{ei}^{\rm D\,\dagger} Y_{ie}^{\rm D} \, \gamma_{av} \, T_{\rm EW} < H(T_{\rm EW}) \,. \tag{4.6}$$

Here the dimensionless quantities $\gamma_{av} \approx 3 \times 10^{-3}$ are derived from the decay rates of the right-handed neutrino N_e of the 'electron flavour' tabulated in Ref. [50]. These right-handed neutrino decay (or equivalently production) rates were computed in [50] using $1 \leftrightarrow 2$ and $2 \leftrightarrow 2$ processes[2] involving the neutrino vertices $Y_{ai}^{D\dagger} \overline{l_{La}} (\varepsilon H)^\dagger N_i$ and $Y_{ia}^D \overline{N_i} (\varepsilon H) l_{La}$ with the Dirac Yukawas.

---

[2]These processes are shown in Figs. 1 and 2 in Ref. [50] and contain a single external N leg – as relevant for the N-production or decay processes of interest.
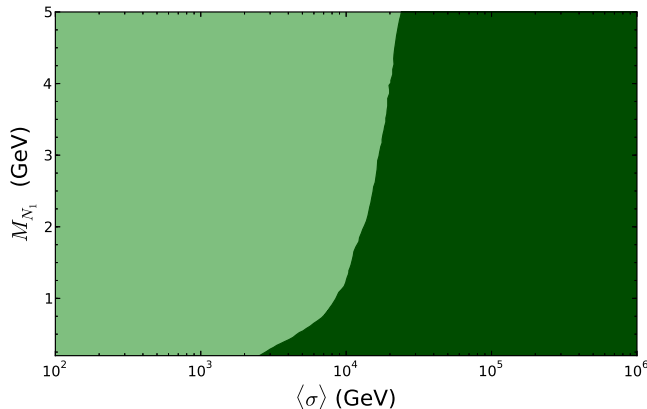
Figure 9: The region in dark green can explain the baryon asymmetry through leptogenesis; we have fixed the mass splittings to be $\Delta M_{N_i} \geq M_{N_1}/10$. This plot shows that there is a lower bound $\langle\sigma\rangle > 2.5$ TeV in order to produce the correct amount of baryon asymmetry. The region in light green cannot produce enough baryon symmetry and/or does not satisfy the wash-out criterion Eq. (4.6).

One can also ask if the new interactions present in our model, those involving the Majorana Yukawas, $\frac{1}{2} Y^M_{ij} \sigma \overline{N}^c_i N_j$ and $\frac{1}{2} Y^{M\dagger}_{ij} \sigma \overline{N}_i N^c_j$, could affect the dynamics. These interactions always contain a pair of right-handed neutrinos and do not change the right-handed neutrino number (the singlet σ carries the N-number -2 but above the electroweak phase transition temperature, the vev of σ vanishes). Hence these processes could contribute to the N production or decay into the Standard Model particles only in combination with other interactions. As the Majorana Yukawa couplings are small $Y^M \approx 10^{-5}$ on the part of the parameter space relevant for us (see Table 3) and the cross-section being proportional to $(Y^M)^2$ means that these interactions will give subleading effects to all the processes considered in [50]. Therefore, we can follow [12] and make the assumption that the number density of sterile neutrinos is very small compared to their equilibrium density at high temperatures, $T_{\text{osc}} \approx 10^6$ GeV, around which the main contributions to the lepton-flavour asymmetry are generated.

It was already shown in [6] that flavoured leptogenesis can work in a classically scale invariant framework. In their set-up three right-handed neutrinos are coupled to a scalar field that acquires a vev, as in the present model. The main difference being that in the present scenario we have not gauged the $B-L$ quantum number. We quote the final result for the lepton flavour asymmetry (of ath flavour) obtained in [6] from extending the results of Ref. [12] to the classically scale-invariant case,

$$\frac{n_{La}}{s} = -\gamma^2_{av} \times 7.3 \times 10^{-4} \sum_c \sum_{i\neq j} i\,(Y^{\mathrm{D}\dagger}_{ai} Y^{\mathrm{D}}_{ic} Y^{\mathrm{D}\dagger}_{cj} Y^{\mathrm{D}}_{ja} - Y^{\mathrm{D}\,\mathrm{t}}_{ai} Y^{\mathrm{D}*}_{ic} Y^{\mathrm{D}\,\mathrm{t}}_{cj} Y^{\mathrm{D}*}_{ja}) \times \mathcal{I}_{ij}\,, \quad (4.7)$$

where the quantity $\mathcal{I}_{ij}$ is given by,

$$\mathcal{I}_{ij} = \frac{16}{\sum_k (Y^{\mathrm{M}\dagger}_{ik} Y^{\mathrm{M}}_{ki} - Y^{\mathrm{M}\dagger}_{jk} Y^{\mathrm{M}}_{kj})} \frac{M_{\mathrm{P}}}{\langle\sigma\rangle} \left(1 - \frac{\langle\sigma\rangle}{T_{\text{osc}}} + \frac{1}{4}\tan^{-1}\left(\frac{4\langle\sigma\rangle}{T_{\text{EW}}}\right) - \frac{1}{4}\tan^{-1}(4)\right)\,, \quad (4.8)$$

for $\langle\sigma\rangle < T_{\rm osc}$. For the case $\langle\sigma\rangle \geq T_{\rm osc}$ and further details on the derivation of Eq. (4.7) we refer the reader to Ref. [6]. It follows from (4.8) that the amount of the lepton flavour asymmetry is proportional to $\langle\sigma\rangle M_P/\Delta M_{N_i}^2$. Hence if we want to avoid any excessive fine-tuning of the mass splittings between different flavours of Majorana neutrinos, the relatively large values of $\langle\sigma\rangle \gtrsim 10^4$ GeV are preferred. From Fig. 9 we can see that there is a lower bound on $\langle\sigma\rangle$ if we impose some restriction on the mass splittings of the right-handed neutrinos. In view that we would like to stay far away from the fine-tuning region, we impose $\Delta M_{N_i} \geq M_{N_1}/10$ which gives the limit $\langle\sigma\rangle > 2.5$ TeV in order for leptogenesis to explain the baryon asymmetry. Imposing this condition removes the points with very small mixing angle γ, as can be seen in the left panel of Fig. 6.

As we can see from Fig. 9 there is also an upper bound on M_{N_i} for each value of $\langle\sigma\rangle$, this bound is mainly due to the wash-out criterion Eq. (4.6) not being satisfied any more. This upper bound becomes weaker once we reach $\langle\sigma\rangle \geq 10^4$ GeV. This sits well with our approach based on the common dynamical origin of all vevs: once an explanation for dark matter is included, $\langle\sigma\rangle$ cannot be too large compared to $\langle\phi\rangle$.

The procedure to obtain the plot in Fig. 9 is as follows. We fix the complex phases ω_{12} and ω_{13} to the benchmark values given in [12] ($\omega_{12} = 1 + 2.6i$ and $\omega_{13} = 0.9 + 2.7i$), and for each point we scan over ω_{23}, if we find at least one point that works well then we label it as a good point (dark green) otherwise it is a bad point (light green). In further scans we have found that varying ω_{12} and ω_{13} has a negligible impact on the final results.

The generated total lepton asymmetry is proportional to $\langle\sigma\rangle$, (cf. (4.7), (4.8))

$$n_L \sim (Y^D)^4 \frac{\langle\sigma\rangle M_P}{\Delta M_{N_i}^2} \sim \langle\sigma\rangle M_P \frac{m_\nu^2}{v^4}\,, \tag{4.9}$$

where we used the see-saw mechanism for the masses m_ν of visible neutrinos, and v is the SM Higgs vev. Hence n_L vanishes as $\langle\sigma\rangle$ approaches zero. This also explains why in Fig. 9, there is a stronger dependence on $\langle\sigma\rangle$ than on the masses M_{N_i}.

We carried out a scan over all free parameters in our model to determine the region of the parameter space where the leptogenesis mechanism outlined above can generate the observed baryon asymmetry. At the same time we require that the model provides a viable candidate for cosmological dark matter. We would like to mention in passing that all the present results on leptogenesis also hold when a generic scalar generates a mass for the sterile neutrinos (i.e with no reference to classical scale invariance).

The results of the scan and the connection between the leptogenesis and dark matter scales are reviewed in the following Section. Furthermore, in Tables 2 and 3 we present four benchmark points to illustrate the viable model parameters. In the remainder of this Section we would like to comment on the choice of parameters for the leptogenesis part of the story.

We first note that our leptogenesis realisation does not require any sizeable fine-tuning of the mass splittings ΔM_{N_i}. For example our first benchmark point BP 1 has (cf. Table 3),

$$M_N = (0.225\,, 0.25\,, 0.275)\,{\rm GeV}. \tag{4.10}$$

At the same time, the masses of active neutrinos are set to agree with the observed mass splittings; for BP 1 we have,

$$m_\nu = (0\,,\, 8.7\,,\, 49.0)\,\text{meV}. \tag{4.11}$$

The lepton asymmetry (4.7) also depends on the matrix of Dirac Yukawa couplings Y^D. We compute Y^D in the Casas-Ibarra parametrisation Eq. (4.2) using (4.10) and (4.11) along with the PMNS matrix and the $\mathcal{R}$ matrix. We have carried out a general scan on the complex angles ω_{ij} of the $\mathcal{R}$ matrix and found that having non-vanishing $\text{Im}[\omega_{ij}]$ is important in order to obtain the required amount of lepton asymmetry.[3] At the same time this does not lead to any excessive fine-tuning. We have checked this for the numerical values of $\mathcal{R}$ matrix elements in our scan. For example, for BP 1 we have (using the ω_{ij} values in Table 3),

$$\mathcal{R} = \begin{pmatrix} -36.52 - 33.80i & 34.11 - 36.97i & 5.854 + 4.604i \\ 84.43 + 100.0i & -101.0 + 85.98i & -16.63 - 14.20i \\ -105.4 + 91.81i & -93.42 - 106.4i & 14.94 - 17.61i \end{pmatrix}, \tag{4.12}$$

and the resulting matrix of Dirac Yukawa couplings,

$$Y^D = \begin{pmatrix} 17.87 - 2.12i & -73.37 - 125.6i & -210.9 - 127.3i \\ -2.168 - 19.11i & -134.4 + 77.79i & -136.9 + 224.6i \\ -3.395 - 0.2434i & 9.677 + 24.56i & 34.69 + 28.93i \end{pmatrix} \times 10^{-8}. \tag{4.13}$$

These matrices do not exhibit a high degree of tuning, and we have checked that this is also the case for generic points of our scan.

5 Connection among the scales

After having performed a scan over all free parameters in our model, we find that:
(1) $\langle\phi\rangle < 17$ TeV in order for dark matter not to overclose the universe, and
(2) $\langle\sigma\rangle > 2.5$ TeV in order in order for leptogenesis to explain the baryon asymmetry.

From the left plot of Fig. 6 we can see that the interesting region in parameter space has large values of $\sin\gamma$, and with this in mind we can separate the interesting regime into two regions:

1. $\langle\sigma\rangle \approx \langle\phi\rangle \sim$ TeV
   In this region[4] we have $\sin\gamma \approx \cos\gamma$ ($\gamma \approx \pi/4$) so there is a strong mixing between the scalar states ϕ and σ, and due to the Gildener-Weinberg conditions $\lambda_\phi \approx \lambda_\sigma$. To avoid overproducing DM, both $\langle\sigma\rangle$ and $\langle\phi\rangle$ have to be less than 10 TeV. Due to the not so large values of $\langle\sigma\rangle$, a large part of this region requires some amount of fine-tuning of the right-handed neutrino mass splittings in order for leptogenesis to work. The use of the Gildener-Weinberg mechanism is crucial in this region.

---

[3]Note that positive values of $\text{Im}[\omega_{ij}]$ enhance the elements of the Dirac Yukawa matrix Y^D.
[4]Recall that $\tan^2\gamma = \langle\sigma\rangle^2/\langle\phi\rangle^2$.

	BP 1	BP 2	BP 3	BP 4
Ωh^2	0.122	0.12	0.12	0.118
σ_{SI} (cm^2)	1.90×10^{-46}	3.32×10^{-46}	1.06×10^{-46}	3.11×10^{-47}
$\langle h \rangle$ (GeV)	246	246	246	246
$\langle \phi \rangle$ (GeV)	2260	1260	1020	4590
$\langle \sigma \rangle$ (GeV)	3080	5930	2830	11790
$\lambda_{h\phi}$	0.035	0.406	-0.335	0.017
$\lambda_{\phi\sigma}$	0.164	0.122	0.40	0.141
$\lambda_{h\sigma}$	0.0185	0.018	-0.045	0.003
λ_h	0.131	0.159	0.147	0.130
λ_σ	0.044	0.003	0.027	0.011
λ_ϕ	0.152	1.352	1.527	0.464
g_{DM}	0.61	1.39	0.96	2.41
M_{h_1} (GeV)	125	125	125	125
M_{h_2} (GeV)	81.6	94.1	137.3	839.1
M_{h_3} (GeV)	1544	2124	1900	4745
$M_{Z'}$ (GeV)	690	880	490	5527
$\sin\alpha$	0.06	0.04	0.08	0.02
$\sin\beta$	0.01	0.03	-0.025	0.001
$\sin\gamma$	0.80	0.98	0.94	0.93
μ_{GW} (GeV)	829	1149	1110	4550

Table 2: Four benchmark points for the model presented in this work. All four points give the correct dark matter abundance within 2σ.

2. $\langle\sigma\rangle \gg \langle\phi\rangle \sim \mathrm{TeV}$

In this region we have $\sin\gamma \approx 1$, so it can be seen as the Coleman-Weinberg limit of the more general Gildener-Weinberg mechanism. The scalar σ overlaps maximally with h_2 and can be thought of as the Coleman-Weinberg scalar. In this region the radiative symmetry breaking is induced by $\lambda_\sigma \ll 1$ and we get $M_{h_2} \ll M_{h_3}$. This region also corresponds to the majority of good (blue) points in Figs. 4-6. Most points have $M_{\mathrm{DM}} > M_{h_2}$. This is the region of most interest since the large values of $\langle\sigma\rangle$ require almost no fine-tuning in ΔM_{N_i} in order for leptogenesis to work.

In Table 2 we give a set of benchmark points that satisfy all experimental constraints and give the correct dark matter abundance within 2σ. The benchmark points BP1, BP2 and BP3 are within reach of future direct detection dark matter experiments. For these same points we provide in Table 3 numerical values that generate the correct amount of baryon asymmetry via leptogenesis. We work with the current experimental central values for the neutrino sector taken from [51], we assume normal ordering for the active neutrino masses. The values for $\langle Y^D \rangle$ are computed as the average of $\sqrt{2M_N m_\nu}/\langle h \rangle$. This estimate corresponds to the naive see-saw relation and it is smaller than the actual entries in the matrix Y^D due to the enhancement by the imaginary parts of ω_{ij} in the $\mathcal{R}$ matrix.

	BP 1	BP 2	BP 3	BP 4
$\langle \sigma \rangle$ (GeV)	3080	5930	2830	11790
M_{N_1} (GeV)	0.225	0.30	0.20	0.9
M_{N_2} (GeV)	0.25	0.33	0.22	1.0
M_{N_3} (GeV)	0.275	0.36	0.24	1.1
m_1 (meV)	0.0	0.0	0.0	0.0
m_2 (meV)	8.7	8.7	8.7	8.7
m_3 (meV)	49.0	49.0	49.0	49.0
$\sin \theta_{12}$	0.55	0.55	0.55	0.55
$\sin \theta_{23}$	0.67	0.67	0.67	0.67
$\sin \theta_{13}$	0.15	0.15	0.15	0.15
δ	$-\pi/4$	-0.6	$-\pi/4$	π
α_1	0	0.3	0	$-\pi$
α_2	$-\pi/2$	-1.1	$-\pi/2$	π
ω_{12}	$1.5 + 2.6i$	$1.5 + 2.6i$	$1.0 + 2.6i$	$1.5 + 2.6i$
ω_{13}	$0.9 + 2.7i$	$0.9 + 2.7i$	$0.9 + 2.7i$	$0.9 + 2.7i$
ω_{23}	$0.03 - 1.8i$	$-0.30 - 1.4i$	$0.05 - 1.85i$	$-1.4i$
$n_{Le}/(s \times 2.5 \times 10^{-10})$	-4.71	-5.75	-5.36	-6.43
$n_{L\mu}/(s \times 2.5 \times 10^{-10})$	-1.66	-44.18	19.03	-75.82
$n_{L\tau}/(s \times 2.5 \times 10^{-10})$	6.37	49.93	-13.67	82.25
$\Gamma_e/H(T_{\mathrm{EW}})$	0.90	0.82	0.91	0.98
$\Gamma_\mu/H(T_{\mathrm{EW}})$	58.43	42.29	56.61	315.5
$\Gamma_\tau/H(T_{\mathrm{EW}})$	167.63	99.03	163.07	115.56
T_{osc} (GeV)	4.43×10^6	1.90×10^6	3.71×10^6	4.84×10^6
Y_1^{M}	7.3×10^{-5}	5.1×10^{-5}	7.1×10^{-5}	7.6×10^{-5}
Y_2^{M}	8.1×10^{-5}	5.6×10^{-5}	7.8×10^{-5}	8.5×10^{-5}
Y_3^{M}	8.9×10^{-5}	6.1×10^{-5}	8.5×10^{-5}	9.4×10^{-5}
$\langle Y^{\mathrm{D}} \rangle$	1.26×10^{-8}	1.45×10^{-8}	1.18×10^{-8}	2.5×10^{-8}

Table 3: Parameters for leptogenesis, same benchmark points as in Table 2.

Nevertheless, for our benchmark points these enhancement factors are always less than 1.5×10^2.

Finding a connection between the scale $\langle \phi \rangle$, responsible for dark matter, and the scale $\langle \sigma \rangle$, responsible for leptogenesis, would be of high interest. From Eq. (4.7) and applying the conversion factor (4.3), we can approximate the baryon relic abundance as,

$$\Omega_b h^2 \approx 2.045 \, M_{\mathrm{P}} \frac{\Delta(Y_D^4) \langle \sigma \rangle}{\Delta(M_N^2)} \, . \tag{5.1}$$

Regarding the dark matter relic density, in a large portion of our parameter scan semi-annihilations are dominant over annihilations, and hence we can approximate by,

$$\Omega_{\mathrm{DM}} h^2 \approx \frac{1.07 \times 10^9 \, x_f}{\sqrt{g_\star} \, M_{\mathrm{P}} \, 2 \langle \sigma_{abc} v \rangle /3} \times \mathrm{GeV}^{-1} \, , \tag{5.2}$$
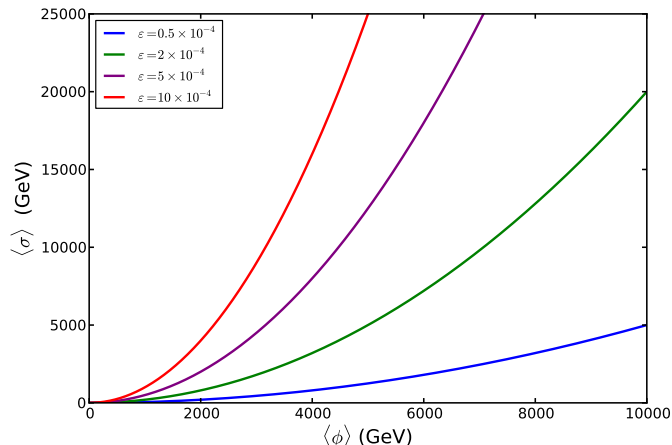
Figure 10: Relation among the two vacuum expectation values, $\langle\phi\rangle$ and $\langle\sigma\rangle$, that yields the observed value of $\Omega_{\mathrm{DM}}h^2/\Omega_b h^2 = 5$. Different colours correspond to different values of the parameter ε defined in Eq. (5.6).

where $x_f = M_{Z'}/T_f$, T_f is the freeze-out temperature for dark matter, and $g_\star$ is the effective number of relativistic degrees of freedom. A good approximation for the mixing angles is to take $\alpha \approx \beta \approx 0$ and $\sin\gamma \approx 0.9$, substituting these values into Eq. (3.1) leads to,

$$\Omega_{\mathrm{DM}}h^2 \approx \frac{7.76 \times 10^{11}}{M_{\mathrm{P}}} \frac{\langle\phi\rangle^2}{g_{\mathrm{DM}}^2} \times \mathrm{GeV}^{-1}\,. \tag{5.3}$$

Using Eqs.(5.1) and (5.3) we can find the ratio

$$\frac{\Omega_{\mathrm{DM}}h^2}{\Omega_b h^2} \approx \frac{3.79 \times 10^{11} \Delta(M_N^2)}{M_{\mathrm{P}}^2\, g_{\mathrm{DM}}^2\, \Delta(Y_D^4)} \frac{\langle\phi\rangle^2}{\langle\sigma\rangle} \times \mathrm{GeV}^{-1} = 5\,, \tag{5.4}$$

where the last equality comes from the observed relic densities [43]. After imposing this relation we find a connection among the scales in the model,

$$\langle\sigma\rangle \approx \varepsilon \langle\phi\rangle^2 \times \mathrm{GeV}^{-1}\,, \tag{5.5}$$

where the parameter ε is defined as,

$$\varepsilon = \frac{7.59 \times 10^{10} \Delta(M_N^2)}{M_{\mathrm{P}}^2\, g_{\mathrm{DM}}^2\, \Delta(Y_D^4)}\,. \tag{5.6}$$

The parameter M_N has a dependence on $\langle\sigma\rangle$, but from a physical perspective it is more relevant to fix the mass splittings rather than the Majorana Yukawa couplings. The parameter ε gives the connection between both scales, typical values for this parameter are around 10^{-4}. Figure 10 illustrates this connection between the scales keeping the parameter ε fixed to different values.

6 Conclusions

We have presented a model that can explain dark matter and the baryon asymmetry of the universe simultaneously, where all the scales in the theory are dynamically generated and have a common origin.

In order to ensure the stability of the dark matter candidate, one usually needs to introduce a discrete symmetry by hand. One of the attractive features of the present model is that it leads to a stable DM candidate without the need of introducing an extra discrete symmetry. We already know that in the Standard Model lepton number and baryon number are accidental symmetries, the latter being responsible for the stability of the proton. In our framework the hidden vector DM is stable due to the accidental non-Abelian global symmetry SO(3). This accidental symmetry could be broken by non-renormalizable operators leading to the decay of Z'^a and producing an intense gamma-ray line that could be detected in future experiments [52].

The theory also predicts two extra scalar states that have a Higgs-like behaviour and masses around the electroweak scale. From the relation for $\tan^2 \alpha$, Eq. (2.23), the interesting region $\langle \sigma \rangle \gg \langle h \rangle$ already requires a small mixing angle α with the SM Higgs boson, due to the small mixing angles we obtain values of $\cos^2 \alpha \cos^2 \beta > 0.95$, so their detection would only be feasible at future colliders. Nevertheless, the LHC at high luminosity will improve the current constraints on the mixing angles α and β.

From dark matter considerations the value of $\langle \phi \rangle$ is required to be around the TeV scale and due to the common origin of all the vevs, $\langle \sigma \rangle$ cannot be too large, compared to $\langle \phi \rangle$, which means that sterile neutrinos should have small masses of order $\mathcal{O}(1)$ GeV in order for leptogenesis to work without severe tuning of the mass splittings ΔM_{N_i}. Under some mild assumptions, we found a connection among the scales $\langle \phi \rangle$ (responsible for dark matter) and $\langle \sigma \rangle$ (responsible for leptogenesis) Eq. (5.5), in order to match the observed ratio $\Omega_{\mathrm{DM}} h^2 / \Omega_b h^2 = 5$. Using classical scale invariance as an underlying symmetry, we have constructed a minimal extension of the SM that addresses dark matter, the baryon asymmetry of the universe and the origin of the electroweak scale.

Acknowledgments

References

[1] S. R. Coleman and E. J. Weinberg, *Radiative Corrections as the Origin of Spontaneous Symmetry Breaking*, *Phys. Rev.* **D7** (1973) 1888–1910.

[2] W. A. Bardeen, *On naturalness in the standard model*, in *Ontake Summer Institute on Particle Physics Ontake Mountain, Japan, August 27-September 2, 1995*, 1995.

[3] R. Hempfling, *The Next-to-minimal Coleman-Weinberg model*, *Phys. Lett.* **B379** (1996) 153–158, [hep-ph/9604278].

[4] W. F. Chang, J. N. Ng and J. M. S. Wu, *Shadow Higgs from a scale-invariant hidden U(1)(s) model,* Phys. Rev. D **75** (2007) 115016 [hep-ph/0701254].

[5] C. Englert, J. Jaeckel, V. V. Khoze, and M. Spannowsky, *Emergence of the Electroweak Scale through the Higgs Portal*, *JHEP* **04** (2013) 060, [arXiv:1301.4224].

[6] V. V. Khoze and G. Ro, *Leptogenesis and Neutrino Oscillations in the Classically Conformal Standard Model with the Higgs Portal*, *JHEP* **10** (2013) 075, [arXiv:1307.3764].

[7] T. Hambye and A. Strumia, *Dynamical generation of the weak and Dark Matter scale*, *Phys. Rev.* **D88** (2013) 055022, [arXiv:1306.2329].

[8] C. D. Carone and R. Ramos, *Classical scale-invariance, the electroweak scale and vector dark matter,* Phys. Rev. D **88** (2013) 055020 [arXiv:1307.8428].

[9] V. V. Khoze, C. McCabe, and G. Ro, *Higgs vacuum stability from the dark matter portal*, *JHEP* **08** (2014) 026, [arXiv:1403.4953].

[10] A. Karam and K. Tamvakis, *Dark matter and neutrino masses from a scale-invariant multi-Higgs portal*, *Phys. Rev.* **D92** (2015), no. 7 075010, [arXiv:1508.03031].

[11] E. K. Akhmedov, V. A. Rubakov, and A. Yu. Smirnov, *Baryogenesis via neutrino oscillations*, *Phys. Rev. Lett.* **81** (1998) 1359–1362, [hep-ph/9803255].

[12] M. Drewes and B. Garbrecht, *Leptogenesis from a GeV Seesaw without Mass Degeneracy*, *JHEP* **03** (2013) 096, [arXiv:1206.5537].

[13] K. A. Meissner and H. Nicolai, *Conformal Symmetry and the Standard Model*, *Phys. Lett.* **B648** (2007) 312–317, [hep-th/0612165].

[14] R. Foot, A. Kobakhidze, K. McDonald, and R. Volkas, *Neutrino mass in radiatively-broken scale-invariant models*, *Phys. Rev.* **D76** (2007) 075014, [arXiv:0706.1829].

[15] R. Foot, A. Kobakhidze, K. L. McDonald, and R. R. Volkas, *A Solution to the hierarchy problem from an almost decoupled hidden sector within a classically scale invariant theory*, *Phys. Rev.* **D77** (2008) 035006, [arXiv:0709.2750].

[16] S. Iso, N. Okada, and Y. Orikasa, *Classically conformal $B^- L$ extended Standard Model*, *Phys. Lett.* **B676** (2009) 81–87, [arXiv:0902.4050].

[17] M. Holthausen, M. Lindner, and M. A. Schmidt, *Radiative Symmetry Breaking of the Minimal Left-Right Symmetric Model*, *Phys. Rev.* **D82** (2010) 055002, [arXiv:0911.0710].

[18] L. Alexander-Nunneley and A. Pilaftsis, *The Minimal Scale Invariant Extension of the Standard Model*, *JHEP* **09** (2010) 021, [arXiv:1006.5916].

[19] J. S. Lee and A. Pilaftsis, *Radiative Corrections to Scalar Masses and Mixing in a Scale Invariant Two Higgs Doublet Model*, *Phys. Rev.* **D86** (2012) 035004, [arXiv:1201.4891].

[20] M. Heikinheimo, A. Racioppi, M. Raidal, C. Spethmann, and K. Tuominen, *Physical Naturalness and Dynamical Breaking of Classical Scale Invariance*, *Mod. Phys. Lett.* **A29** (2014) 1450077, [arXiv:1304.7006].

[21] A. Farzinnia, H.-J. He, and J. Ren, *Natural Electroweak Symmetry Breaking from Scale Invariant Higgs Mechanism*, *Phys. Lett.* **B727** (2013) 141–150, [arXiv:1308.0295].

[22] V. V. Khoze, *Inflation and Dark Matter in the Higgs Portal of Classically Scale Invariant Standard Model*, *JHEP* **11** (2013) 215, [arXiv:1308.6338].

[23] E. Gabrielli, M. Heikinheimo, K. Kannike, A. Racioppi, M. Raidal, and C. Spethmann, *Towards Completing the Standard Model: Vacuum Stability, EWSB and Dark Matter*, *Phys. Rev.* **D89** (2014), no. 1 015017, [arXiv:1309.6632].

[24] C. Tamarit, *Running couplings with a vanishing scale anomaly*, *JHEP* **12** (2013) 098, [arXiv:1309.0913].

[25] S. Abel and A. Mariotti, *Novel Higgs Potentials from Gauge Mediation of Exact Scale Breaking*, *Phys. Rev.* **D89** (2014), no. 12 125018, [arXiv:1312.5335].

[26] K. Allison, C. T. Hill, and G. G. Ross, *Ultra-weak sector, Higgs boson mass, and the dilaton*, *Phys. Lett.* **B738** (2014) 191–195, [arXiv:1404.6268].

[27] S. Benic and B. Radovcic, *Majorana dark matter in a classically scale invariant model*, *JHEP* **01** (2015) 143, [arXiv:1409.5776].

[28] A. D. Plascencia, *Classical scale invariance in the inert doublet model*, *JHEP* **09** (2015) 026, [arXiv:1507.04996].

[29] K. Ghorbani and H. Ghorbani, *Scalar Dark Matter in Scale Invariant Standard Model*, *JHEP* **04** (2016) 024; [arXiv:1511.08432].

[30] A. Ahriche, A. Manning, K. L. McDonald, and S. Nasri, *Scale-Invariant Models with One-Loop Neutrino Mass and Dark Matter Candidates*, arXiv:1604.05995.

[31] T. Hambye, *Hidden vector dark matter*, *JHEP* **01** (2009) 028, [arXiv:0811.0172].

[32] C. Gross, O. Lebedev, and Y. Mambrini, *Non-Abelian gauge fields as dark matter*, *JHEP* **08** (2015) 158, [arXiv:1505.07480].

[33] S. Di Chiara and K. Tuominen, *A minimal model for SU(N) vector dark matter*, *JHEP* **11** (2015) 188, [arXiv:1506.03285].

[34] V. V. Khoze and G. Ro, *Dark matter monopoles, vectors and photons*, *JHEP* **10** (2014) 61, [arXiv:1406.2291].

[35] E. Gildener and S. Weinberg, *Symmetry Breaking and Scalar Bosons*, *Phys. Rev.* **D13** (1976) 3333.

[36] S. P. Martin, *Two loop effective potential for a general renormalizable theory and softly broken supersymmetry*, *Phys. Rev.* **D65** (2002) 116003, [hep-ph/0111209].

[37] V. Martín Lozano, J. M. Moreno, and C. B. Park, *Resonant Higgs boson pair production in the $hh \to b\bar{b}\, WW \to b\bar{b}\ell^+\nu\ell^-\bar{\nu}$ decay channel*, *JHEP* **08** (2015) 004, [arXiv:1501.03799].

[38] T. Robens and T. Stefaniak, *Status of the Higgs Singlet Extension of the Standard Model after LHC Run 1*, *Eur. Phys. J.* **C75** (2015) 104, [arXiv:1501.02234].

[39] A. Falkowski, C. Gross, and O. Lebedev, *A second Higgs from the Higgs portal*, *JHEP* **05** (2015) 057, [arXiv:1502.01361].

[40] J. A. Casas and A. Ibarra, *Oscillating neutrinos and muon —> e, gamma*, *Nucl. Phys.* **B618** (2001) 171–204, [hep-ph/0103065].

[41] C. Boehm, M. J. Dolan, and C. McCabe, *A weighty interpretation of the Galactic Centre excess*, *Phys. Rev.* **D90** (2014), no. 2 023531, [arXiv:1404.4977].

[42] G. Belanger, F. Boudjema, A. Pukhov, and A. Semenov, *MicrOMEGAs: A Program for calculating the relic density in the MSSM*, *Comput. Phys. Commun.* **149** (2002) 103–120, [`hep-ph/0112278`].

[43] **Planck** Collaboration, P. A. R. Ade et al., *Planck 2015 results. XIII. Cosmological parameters*, `arXiv:1502.01589`.

[44] **LUX** Collaboration, D. S. Akerib et al., *First results from the LUX dark matter experiment at the Sanford Underground Research Facility*, *Phys. Rev. Lett.* **112** (2014) 091303, [`arXiv:1310.8214`].

[45] D. C. Malling et al., *After LUX: The LZ Program*, `arXiv:1110.0103`.

[46] J. Billard, L. Strigari, and E. Figueroa-Feliciano, *Implication of neutrino backgrounds on the reach of next generation dark matter direct detection experiments*, *Phys. Rev.* **D89** (2014), no. 2 023524, [`arXiv:1307.5458`].

[47] S. Baek, P. Ko, W.-I. Park, and E. Senaha, *Higgs Portal Vector Dark Matter : Revisited*, *JHEP* **05** (2013) 036, [`arXiv:1212.2131`].

[48] E. Aprile *et al.* [XENON Collaboration], *Physics reach of the XENON1T dark matter experiment,* JCAP **1604** (2016) no.04, 027 [`arXiv:1512.07501`].

[49] B. Shuve and I. Yavin, *Baryogenesis through Neutrino Oscillations: A Unified Perspective*, *Phys. Rev.* **D89** (2014), no. 7 075014, [`arXiv:1401.2459`].

[50] D. Besak and D. Bodeker, *Thermal production of ultrarelativistic right-handed neutrinos: Complete leading-order results,* JCAP **1203** (2012) 029. [`arXiv:1202.1288`].

[51] M. C. Gonzalez-Garcia, M. Maltoni, and T. Schwetz, *Updated fit to three neutrino mixing: status of leptonic CP violation*, *JHEP* **11** (2014) 052, [`arXiv:1409.5439`].

[52] C. Arina, T. Hambye, A. Ibarra, and C. Weniger, *Intense Gamma-Ray Lines from Hidden Vector Dark Matter Decay*, *JCAP* **1003** (2010) 024, [`arXiv:0912.4496`].